

# Extraordinary optical absorption through subwavelength slits

Justin S. White,<sup>1</sup> Georgios Veronis,<sup>2</sup> Zongfu Yu,<sup>3</sup> Edward S. Barnard,<sup>1</sup>  
Anu Chandran,<sup>1</sup> Shanhui Fan,<sup>3</sup> and Mark L. Brongersma<sup>1,\*</sup>

<sup>1</sup>Geballe Laboratory for Advanced Materials, Stanford, California 94305, USA

<sup>2</sup>Department of Electrical and Computer Engineering, Louisiana State University, Baton Rouge, Louisiana 70803, USA

<sup>3</sup>Ginzton Laboratory, Stanford, California 94305, USA

\*Corresponding author: brongersma@stanford.edu

Received December 5, 2008; revised January 23, 2009; accepted January 26, 2009;  
posted February 2, 2009 (Doc. ID 105000); published February 27, 2009

We report on the ability of resonant plasmonic slits to efficiently concentrate electromagnetic energy into a nanoscale volume of absorbing material placed inside or directly behind the slit. This gives rise to extraordinary optical absorption characterized by an absorption enhancement factor that well exceeds the enhancements seen for extraordinary optical transmission through slits. A semianalytic Fabry–Perot model for the resonant absorption is developed and shown to quantitatively agree with full-field simulations. We show that absorption enhancements of nearly 1000% can be realized at 633 nm for slits in aluminum films filled with silicon. This effect can be utilized in a wide range of applications, including high-speed photodetectors, optical lithography and recording, and biosensors. © 2009 Optical Society of America  
OCIS codes: 240.6680, 260.3910, 260.5740.

Since the first observation of extraordinary optical transmission (EOT) through subwavelength apertures in optically thick metal films [1], there has been an explosion of interest in the unusual properties of resonant metallic (i.e., plasmonic) structures. The fundamental physics behind EOT has been extensively studied [2] and a wide range of applications has appeared, including compact color and polarization sensitive filters [3], novel optical lenses [4], and integrated components for the sensor and optoelectronics industries [5]. Subwavelength apertures have also been used to efficiently concentrate light into deep subwavelength regions; most notably, this has enabled modern optical characterization tools such as the scanning near-field optical microscope [6]. More recently, the highly concentrated fields near resonant apertures and particles have been exploited to locally induce strong light absorption by small molecules, polymers, oxides, and semiconductor materials. This type of locally enhanced absorption has enabled single molecule studies of diffusion dynamics [7], nanoscale optical recording [8] and lithography [9], heat-assisted magnetic recording (HAMR) [10] and nanostructure growth [11], and ultrasensitive photodetectors [12–14]. By combining enhanced absorption and emission processes in slits, novel nanoscale light sources can be realized as well [15].

In this Letter, we analyze one of the key plasmon-resonant structures to induce light concentration and absorption enhancements in a deep subwavelength volume: a single isolated slit in a metallic film on an absorbing substrate [see inset of Fig. 1(a)]. As a specific example, we discuss full-field finite-difference frequency-domain (FDFD) simulations [16] of slits generated in an Al film on a Si substrate. Figure 1(a) shows the energy density distribution of a 50-nm-wide, 100-nm-long slit illuminated from the top with a 633 nm plane wave, polarized in the  $x$  direction. Substantial electromagnetic energy concen-

tration is observed both laterally below the diffraction limit as well as into the semiconductor below the absorption depth ( $\sim 3.5 \mu\text{m}$  at  $\lambda = 633 \text{ nm}$ ).

We argue that the enhanced energy density below the slit arises through the resonant excitation of the fundamental field-symmetric surface plasmon-polariton (SPP) mode supported by the slit [see Fig. 1(b)], which behaves as a truncated metal–dielectric–metal (MDM) plasmonic waveguide [17]. Truncation of such a waveguide results in strong reflections from the slit terminations and gives rise to resonant cavity behavior. We develop an intuitive semianalytic Fabry–Perot model to predict the properties of the cavity resonances and to quantify the associated local absorption enhancement and degree of spatial confinement of the electromagnetic energy. We propose a simple-to-fabricate geometry that provides absorption enhancements up to 352% for  $\lambda = 633 \text{ nm}$  illumination as well as a more intricate design with enhancements approaching 1000%.

To enable the construction of an intuitive model for the enhanced light absorption behind a slit, we first quantify the absorption enhancement in a nanoscale

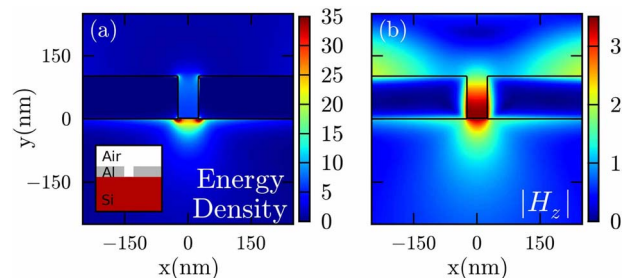


Fig. 1. (Color online) (a) Field energy density for a single isolated slit of 50 nm width in a 100-nm-thick aluminum film on a silicon substrate, top-illuminated by a  $\lambda = 633 \text{ nm}$  plane wave polarized in the  $x$  direction. (b) Magnetic field distribution for the same structure.

$1.5w \times 50$  nm ( $W \times H$ ) region of silicon—where  $w$  is the slit width—directly beneath the slit using FDFD simulations [see Fig. 2(b)]. Figure 2(a) shows the absorption in this region as a function of slit length for several slit widths, normalized to the absorption in the same region of bare silicon without any metallic structure; if a perfect antireflection coating is added to the bare silicon, the absorption enhancement factor would decrease by 34.8%. The observed length dependence is qualitatively similar to that seen for EOT, which was successfully described with a Fabry–Perot resonator model [18], inspiring us to construct a similar model for extraordinary optical absorption (EOA).

To develop a Fabry–Perot model for the absorption enhancement, we examine the fundamental scattering coefficients of the MDM system [Fig. 2(b)]. A plane wave with its electric field polarized normal to the slit ( $x$  direction) is incident from the top of region 1 (dielectric constant  $\epsilon_1$ ) onto a MDM cavity ( $\epsilon_2$ ) of width  $w$  and length  $L$  formed in a metal film ( $\epsilon_M$ ). The plane wave couples into the field-symmetric gap plasmon mode supported by the slit with a transmission coefficient  $t_{12}$ . For the narrow slit widths considered here, this is the only allowed mode. The plane wave also couples to SPPs on the  $\epsilon_1/\epsilon_M$  interface and reflected far-field radiation, but they do not interact further with the isolated slit and can be neglected. The propagating gap plasmon undergoes multiple reflections at the top and bottom interfaces described by complex reflection coefficients  $r_{21}$  and  $r_{23}$ , respectively, which include a magnitude and phase:  $r = |r|e^{i\phi}$ . Finally, the downward propagating gap plasmon mode is outcoupled to induce local absorption described by a coupling coefficient  $\kappa_{23}$ , which is defined as the ratio of the absorption in the  $1.5w \times 50$  nm region directly beneath the slit to the magnitude of the  $E_x$  field of the downward propagating MDM mode. The transmission, reflection, and outcoupling coefficients can be determined analytically via mode-overlap integrals [19] or numerically with FDFD simulations, as is done here. Using the numerically computed scattering coefficients, a phased sum of the directly launched and multiply reflected gap plasmons can be performed to produce a semi-

analytic equation for the absorption in this subwavelength region,

$$\text{Absorption} = \frac{\kappa_{23}|t_{12}|^2 e^{-2|k''_{\text{MDM}}|L}}{|1 - r_{21}r_{23}e^{2ik_{\text{MDM}}L}|^2}, \quad (1)$$

where  $k_{\text{MDM}} = k'_{\text{MDM}} + ik''_{\text{MDM}}$  is the complex wave vector of the gap plasmon mode.

As can be seen from Eq. (1), the MDM slit will be on resonance and the absorption will be maximized when the denominator is minimized; this occurs when  $\phi_{21} + \phi_{23} + 2k'_{\text{MDM}}L = 2m\pi$ , where  $m$  is an integer and gives the order of the resonance. The solid curves in Fig. 2(a) show the excellent agreement of the proposed semianalytic Fabry–Perot model with full-field simulations (symbols); the model clearly captures the essential physics of the system.

One noteworthy feature in Fig. 2(a) is the almost width-independent location of the first-order resonance at  $L \approx 100$  nm. One would expect the resonant length to decrease with decreasing slit width as  $k_{\text{MDM}}$  increases [17]; however, the phase pickup  $\phi$  on reflection decreases as  $w$  decreases [19], countering this trend and resulting in a nearly constant resonant length. Additionally, owing to the substantial phase pickup on reflection, the lowest-order resonance length of  $L_{\text{res}} \approx \lambda_{\text{MDM}}/5$  is significantly shorter than the value  $L_{\text{res}} = \lambda_{\text{MDM}}/2$  predicted when phase is neglected. This is advantageous because losses in the metal are minimized when  $L$  is small, allowing for energy enhancements exceeding 350% for experimentally realizable feature sizes ( $w = 30$  nm); this is a 34% increase over the far-field transmission enhancement into the silicon of 262% for this structure. If losses in the aluminum film could be eliminated, the absorption enhancement would be an additional 19% ( $w = 100$  nm) to 82% ( $w = 30$  nm) larger.

To gain further insight into the physical origin of these large absorption enhancements, full-field simulations are used to quantify the contributions to the localized energy beneath a 50 nm slit from nonpropagating near fields, SPPs confined to the  $\epsilon_M/\epsilon_3$  interface, and propagating far-field radiation (transmitted light). The numerically calculated fields of a  $w = 50$  nm,  $L = 100$  nm MDM cavity with  $\epsilon_1 = \epsilon_2 = \text{air}$ ,  $\epsilon_M = \text{Al}$ ,  $\epsilon_3 = \text{Si}$  were transformed into  $k$ -space by performing 1D Fourier transforms along the  $x$  direction of the fields at different depths in the substrate. These fields were then filtered in  $k$ -space into propagating radiation ( $k < k_{\text{sub}}$ ), surface plasmon waves ( $0.95k_{\text{SPP}} < k < 1.05k_{\text{SPP}}$ ), and localized near fields (everything else). Finally, the fields were transformed back into real space where the energy distribution for each of the three components could be computed. The results of this analysis are shown in Fig. 3(a), which plots the total integrated field energy from all components in a  $w = 75$ -nm-wide section at different depths below the slit; the energy is normalized to the incident plane wave energy in the same region. The decay away from the slit is slow near the interface owing to confined near fields and SPPs but approaches the more rapid ( $\propto 1/x$ ) decay expected for a

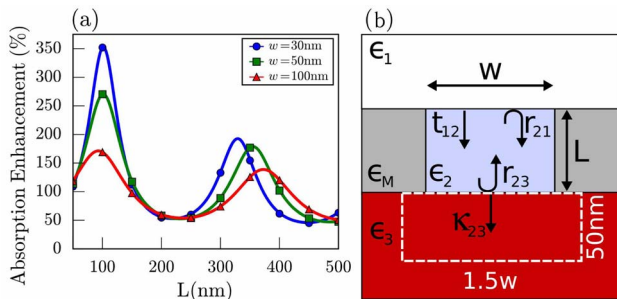


Fig. 2. (Color online) (a) Plot of the absorption enhancement in a nanoscale region directly beneath a slit as a function of MDM cavity length for several widths. The FDFD simulations (symbols) show excellent agreement with the Fabry–Perot model (curves). (b) Schematic showing the relevant scattering coefficients used for the model.

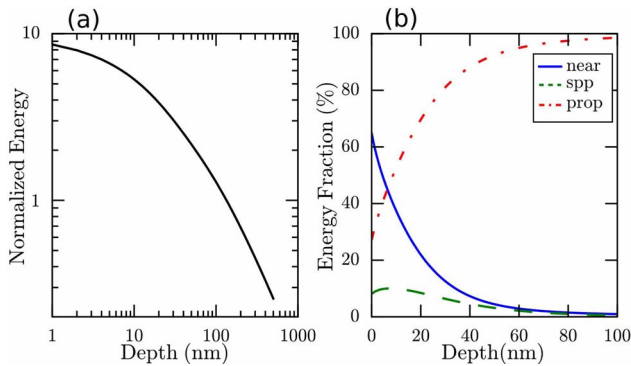


Fig. 3. (Color online) (a) Integrated energy in a  $w = 75$ -nm-wide section at different depths in a Si substrate below a resonant  $w = 50$  nm slit. (b) Relative energy fraction in the near field (solid curve), SPP (dashed curve), and propagating radiation (dashed-dotted curve).

propagating cylindrical wave at larger depths. Figure 3(b) gives the breakdown of this energy into its constituent components, showing that the energy confinement in the first 50 nm is provided largely by the localized near fields and SPPs. In contrast to EOT, EOA can exploit the high-energy densities near the slits, which rapidly fall off in the far field.

Thus far we have considered a simple device geometry with the semiconductor placed beneath the slit in an easy-to-fabricate design; however, this geometry is not optimal, as there is substantial energy confined in the resonant MDM cavity that is not utilized. Figure 4(a) (inset) shows a design with even stronger local field and absorption enhancements [Figs. 4(a) and 4(b)]. The device consists of a free-standing aluminum film with a single isolated slit filled with silicon; the absorption enhancement is relative to the absorption in the same area of a semi-infinite slab of bulk silicon. Figure 4(b) shows the expected Fabry–Perot line shape of absorption enhancement; the semianalytic Fabry–Perot model was also verified with this structure (not shown). This more-optimized structure obtains peak absorption enhancements up to 980%, a substantial improvement over the simpler design.

In summary, we have performed an analysis of EOA within a deep subwavelength region via reso-

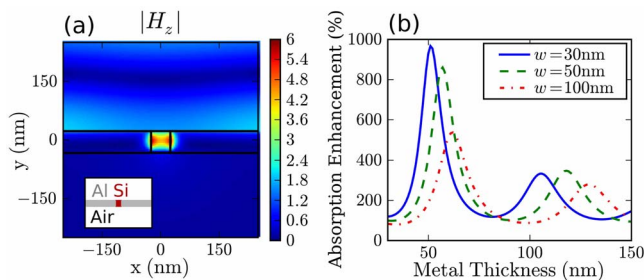


Fig. 4. (Color online) (a) Magnetic field distribution in a  $w = 50$  nm  $\times$   $L = 56$  nm resonant slit filled with Si. (b) Absorption enhancement versus slit length for various slit widths.

nant plasmonic nanostructures. A semianalytic Fabry–Perot model was developed to explain the resonant absorption enhancement and was shown to be in good agreement with full-field FDFD simulations. Fourier  $k$ -space decomposition was used to show that the absorption enhancement results primarily from nonpropagating near fields of the slit and confined surface plasmon waves. Two device geometries were proposed: a simple-to-fabricate device with absorption enhancements exceeding 350% and a more optimized but also more difficult to make device with absorption enhancements approaching 1000%, a tenfold improvement. Such devices have promising applications in high-speed, low-capacitance photodetectors with deep subwavelength active regions as well as efficient nanoscale light sources.

We would like to acknowledge funding support from Northrop Grumman and the United States Air Force Office of Scientific Research (AFOSR).

## References

1. T. W. Ebbesen, H. J. Lezec, H. F. Ghaemi, T. Thio, and P. A. Wolff, *Nature* **391**, 667 (1998).
2. F. J. Garcia de Abajo, *Rev. Mod. Phys.* **79**, 1267 (2007).
3. E. Laux, C. Genet, T. Skauli, and T. W. Ebbesen, *Nat. Photonics* **2**, 161 (2008).
4. L. Verslegers, P. B. Catrysse, Z. Yu, J. S. White, E. Barnard, M. L. Brongersma, and S. Fan, *Nano Lett.* **9**, 235 (2009).
5. C. Genet and T. W. Ebbesen, *Nature* **445**, 39 (2007).
6. E. Betzig and J. K. Trautman, *Science* **257**, 189194 (1992).
7. M. J. Levene, J. Kurlach, S. W. Turner, M. Foquet, H. G. Craighead, and W. W. Webb, *Science* **299**, 682686 (2003).
8. X. Shi and L. Hesselink, *Jpn. J. Appl. Phys. Part 1* **41**, 1632 (2002).
9. L. Wang and X. Xu, *J. Microsc.* **229**, 483 (2008).
10. R. E. Rottmayer, S. Batra, D. Buechel, W. A. Challener, J. Hohlfield, Y. Kubota, L. Li, B. Lu, C. Mihalcea, K. Mountfield, K. Pelhos, C. Peng, T. Rausch, M. A. Seigler, D. Weller, and X. Yang, *IEEE Trans. Magn.* **42**, 2417 (2006).
11. L. Cao, D. N. Barsic, A. R. Guichard, and M. L. Brongersma, *Nano Lett.* **7**, 3523 (2007).
12. T. Ishi, J. Fujikata, K. Makita, T. Babs, and K. Ohashi, *Jpn. J. Appl. Phys. Part 2* **44**, L364 (2005).
13. Z. Yu, G. Veronis, S. Fan, and M. L. Brongersma, *Appl. Phys. Lett.* **89**, 151116 (2006).
14. L. Tang, D. A. B. Miller, A. K. Okyay, J. A. Matteo, Y. Yuen, K. C. Saraswat, and L. Hesselink, *Opt. Lett.* **31**, 1519 (2006).
15. Y. C. Jun, R. D. Kekatpure, J. S. White, and M. L. Brongersma, *Phys. Rev. B* **78**, 153111 (2008).
16. G. Veronis and S. Fan, in *Surface Plasmon Nanophotonics*, M. L. Brongersma and P. G. Kik, eds. (Springer, 2007), Vol. 131, p. 169.
17. R. Zia, M. D. Selkr, P. B. Catrysse, and M. L. Brongersma, *J. Opt. Soc. Am. A* **21**, 2442 (2004).
18. L. Martin-Moreno, F. J. Garcia-Vidal, H. J. Lezec, K. M. Pellerin, T. Thio, J. B. Pendry, and T. W. Ebbesen, *Phys. Rev. Lett.* **86**, 1114 (2001).
19. R. Gordon, *Phys. Rev. B* **73**, 153405 (2006).